Journal of Applied Polymer Science

Jamming Rheology of Model Cementitious Suspensions Composed of Comb-Polymer Stabilized Magnesium Oxide Particles

Lisa R. Murray, Kendra A. Erk
School of Materials Engineering, Purdue University, 701 West Stadium Ave, West Lafayette, Indiana 47907
Correspondence to: K. A. Erk (E-mail: erk@purdue.edu).

ABSTRACT: The colloidal microstructure of concentrated suspensions containing anionic comb-polymer-stabilized magnesium oxide (MgO) particles in water was analyzed by shear rheometry for indications of changes in particle microstructure based on particle size and comb-polymer usage. As the suspensions were sheared at different rates, jamming in the sheared MgO suspensions was observed as shear stress overshoots. The shear-induced evolution of the suspension's microstructure was strongly related to the perceived interactions between neighboring MgO particles in the suspension. In the jammed state, interactions are believed to be enhanced by the formation of entanglements between opposing comb-polymer side-chains. Steric repulsion between side-chains was lessened for large particles on account of their diameters, which further enabled side-chain entanglement during close particle contact under shear. Suspensions with relatively wide particle size distributions (0.5–400 μm) were theorized to form hydrocluster aggregates, while suspensions with narrower particle size distributions (0.5–40 μm) most likely resulted in networked microstructures under the influence of the chain entanglements from the adsorbed comb-polymer. © 2014 Wiley Periodicals, Inc. J. Appl. Polym. Sci. **2014**, *131*, 40429.

KEYWORDS: colloids; rheology; structure-property relations; surfaces and interfaces

Received 4 November 2013; accepted 13 January 2014
DOI: 10.1002/app.40429

INTRODUCTION

Modern cements have attained improved performance through the usage of chemical additives that enhance the mixture stability and workability and lead to improved strength and durability.[1] Polymer superplasticizers have been used for decades in the mixtures of self-compacting cements,[1] typically "polycarboxylates" composed of poly(acrylic-acid) (PAA)[2,3] or poly(methyl methacrylate) (PMMA)-based comb polymers.[4–7] Polycarboxylates have negatively charged backbones with several grafted hydrophilic side-chains, usually polyethylene oxide (PEO),[2,4–8] that absorb to the particle surface [Figure 1(a)] and keep particles stable due to steric stabilization [Figure 1(b)]. The absorption occurs in a basic pH solution with negative charges forming deprotonated carboxylic acid groups. In this manner cementitious mixtures can avoid severe aggregation by the repulsion of the comb-polymer PEO branches, resulting in improved workability and enhanced mechanical properties of the final cured cement product.[1]

Shear rheometry experiments can be applied to quantify the workability of fresh cement during casting and placement. The choice of mechanical characterization in terms of shear is directly relevant to the conditions experienced by cementitious mixtures during processing and pouring. In rheometry experiments, a sample of material is exposed to controlled shear deformation at a fixed shear rate and the resulting shear stress response is measured.

The rheological response of fresh cement to applied shear deformation is directly dependent on the physicochemical structure of the mixture, including parameters such as the concentration of comb-polymer and the oxide particle size distribution. Through shearing the mixtures in a rheometer, shear stress behavior is observed and can be interpreted in terms of the microstructural evolution of particles within the colloid.[9] For example, changes observed in the shear stress response can be driven by particle migration during the duration of the applied shear strain or shear stress. Thus, the particle-polymer interactions of cementitious mixtures can be directly evaluated through controlled rheometry experiments using concentrated suspensions of magnesium oxide (MgO) particles in water as a model system.[1,4,7,10–13]

In rheometry experiments of concentrated particle suspensions, jamming is a common occurrence in which the shear-induced interlocking of neighboring particles results in a local or global barrier to flow.[14] Jamming has been observed in many colloidal suspensions, including silica particles,[15] polymethylmethacrylate particles,[16] bismuth oxychloride (BiOCl),[17] bentonite suspensions,[18] and various polymer melts and solutions.[19,20] The investigation of jamming behavior in model cement suspensions is

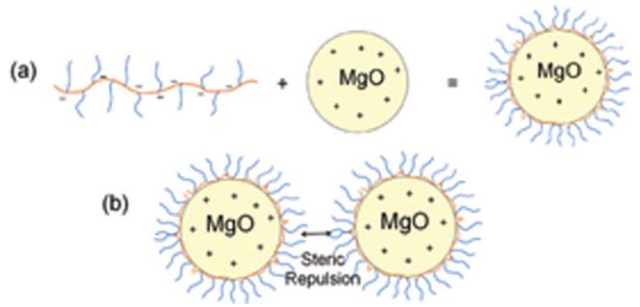

Figure 1. Schematic illustrating the (a) adsorption of a model comb-polymer chain onto a charged MgO particle surface and (b) the steric repulsion between particles because of the presence of the adsorbed comb-polymer. The schematic is not drawn to scale; appropriate dimensions for chains are on the order of nanometer and the size of the particles is on the order of micrometer. [Color figure can be viewed in the online issue, which is available at wileyonlinelibrary.com.]

important for understanding how the adsorbed comb-polymer and solid oxide particles may interact and impact flow under different processing conditions. For example, jamming during cement mixing and processing could be mitigated or avoided by incorporation of next-generation comb-polymer based admixtures in order to produce more workable and stable cements.

In this study, stress responses from controlled shear rheometry experiments of MgO suspensions with different particle size distributions and comb-polymer concentrations display rheological signatures of jamming, including the occurrence of stress maxima during steady shear experiments. Jamming transitions are believed to be influenced by chain entanglement of the comb-polymer side-chains, which cause different particle microstructures based on the choice of the particle size distribution. From these interactions, polymer-stabilized suspensions with narrow particle size distributions are anticipated to form particle networks whereas suspensions with relatively wide particle size distributions promote hydrocluster formation. These theories could be insightful for developing a better understanding of the particle interactions in cement systems containing chemical admixtures.

BACKGROUND

Jamming in cement processing has not been extensively studied because cement rheology typically examines macroscopic rheological behavior separately from the micro-scale particle interactions.[21] Most past work relies on the shear thickening in flow curves as a general measure of particle build-up that tends towards jamming[22,23] or stress or strain amplitude oscillatory shear for signs of jamming.[2,21,24] However, oscillatory measurements are inconsistent with typical cement processing conditions, i.e., pressure-driven shear flow at varying shear rates and large strain magnitudes. In this study, jamming phenomena is assessed through examining data from shear start-up measurements, shear ramp tests, and creep experiments. Each test yields additional insight into the microstructure of the comb-polymer-stabilized particle suspensions.

Typical rheometry investigations of cements pastes and oxide suspensions apply shear ramp experiments, also called "flow curves," to measure the shear stress response (τ) while the shear rate ($\dot{\gamma}$) is increased over time. These experiments show how the sample responds to increasing shear rates as an accumulation of the data from several shear start-up tests, which have a fixed $\dot{\gamma}$. The colloid's low-shear and high-shear behavior during the shear ramp experiment can be viewed on one plot, allowing for shear thinning and shear thickening to be identified. However, due to the history-dependent nature of most concentrated particle suspensions, the shear stress behavior at low and high shear rates captured by a shear ramp experiment typically deviates from the suspension's true shear stress response at a given fixed shear rate. Therefore, multiple shear start-up tests have been utilized here instead of a single shear ramp experiment in order to more accurately quantify the stress response of suspensions that are deformed at different shear rates.

Since the shear rate is fixed during shear start-up experiments, these tests reveal the microstructural behavior of the suspension over long times, typically as it approaches an unchanging, "steady-state" structure which may represent the equilibrium arrangement of the particles[25] or an equilibrium stress.[14] In past work on concentrated colloidal suspensions, it was found that the stress response of the suspension may display a stress overshoot before reaching a steady-state value of shear stress, which is experimentally observed as a shear stress plateau.[25] The plateau regions are believed to have an equilibrium microstructure that maintains a general organization during shearing but does not significantly change the net particle positions over time.[25] On the other hand, stress overshoots are thought to have a dynamic particle microstructure before the steady-state plateau.[14] This rheological and microstructural phenomenon may correspond to the physical interlocking of particles called a "jam" that develops during shear and momentarily hinder or stops flow[14,21] before particles are pushed apart.[26]

Creep experiments apply a constant shear stress (τ) to the sample and record the resulting deformation response in terms of shear strain (γ). They have been used by others to investigate of the setting of cement pastes[27] and to quantify the solid- or liquid-like nature of suspensions.[18,24,28] However, these results have not been understood in terms of the micro-scale particle interactions. Here, creep experiments are performed to simulate the pressure-driven flow of cement during processing and results can be interpreted in terms of microstructural breakdown, either local or global, and with relation to the particle-polymer interactions.

EXPERIMENTAL

Materials

MagChem P-98, a dead-burned magnesium oxide (MgO) powder, was obtained from Martin Marietta Magnesia (Baltimore, MD) and used in two different particle sizes distributions, generally referred to here as the "narrow" and "wide" particle size distribution. Pulverized MagChem P-98 was used as received for the narrow particle size distribution suspensions while MagChem P-98 of mesh size 30 was sieved with a 100 mesh to obtain the wide particle size distribution suspensions. Coulter counter measurements (Coulter LS32 Particle Size Analyzer) gave the particle size distributions for each powder. The MgO

used for the narrow particle size distribution had an average particle diameter of 3.8 μm and a distribution of 0.5–40 μm, with 84.1% of the particles less than 10 μm and merely 0.41% less than 1 μm. The sieved MgO for the wide particle size distribution had an average particle size of 107.2 μm with particle sizes ranging from 0.5 to 400 μm and 48.7% of the particles had diameters less than 100 μm while only 10.2% were smaller than 10 μm. Although the wide size distributions more accurately simulate a Portland cement with particle sizes ranging from 0.001 to 100 μm,[29] most research studies use pulverized MgO particles that are sieved to obtain small, specific size distributions.[4,5,7,11] To create the MgO suspensions, 0.75 weight fraction (0.46 volume fraction, 0.3 weight water/particle ratio) of particles was used in each aqueous suspension of water (deionized by Barnsted nanopure infinity with micron sized filters) to simulate the water-cement weight ratio of 0.3–0.7 and the particle volume fraction of ~0.5 used in cement pastes.[30]

ADVA 190, a high-water-reducing admixture for cement (Grace Construction, Cambridge, MA) composed of polycarboxylate-based comb-polymer, was used as the chemical admixture for MgO suspensions shown in Figure 2, the basic molecular structure of ADVA 190 has a poly(acrylic acid) (PAA) backbone with grafted PEO side-chains. This was confirmed from infrared absorption experiments (Spectrum 100 FTIR with universal attenuated total reflectance sampling accessory) and comparisons with literature.[31]

To remove any low molecular weight species present among the comb-polymer, dialysis was carried out with 12,000 g mol^{-1} cellulose dialysis tubing (Fisher Scientific, Pittsburgh, PA) for three days while changing the water every 8–12 h. Gel permeation chromatography with a Polymer Laboratories PL-GPC20 system and tetrahydrofuran eluent was used to measure the total molecular weight of the dialyzed comb-polymer, which was found to be 20,473 g mol^{-1}. Though the exact molecular structure cannot be directly resolved with GPC, comparisons with literature indicate that a 5,000 g mol^{-1} PAA backbone with 1000 g mol^{-1} PEO side-chains is a common comb-polymer architecture in both commercial comb-polymer studies[11] and custom-synthesized products[6] and yields total molecular weight values of 18,000–23,000 g mol^{-1}.[4]

Methods and Suspension Characterization

Concentrations of ADVA 190 were selected based on the general usage of polycarboxylate superplasticizers in cement pastes. Experiments were conducted within the concentrations of

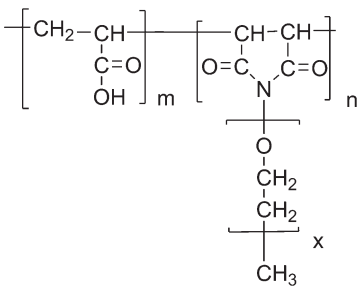

Figure 2. ADVA 190 molecular structure, a poly(acrylic acid) backbone with poly(ethylene oxide) side-chains.

superplasticizer used in cements in order to more accurately correlate the comb-polymer's rheology in MgO to the behavior of cement pastes during processing. The primary concentration of the ADVA 190 used in the MgO suspensions was 6 mg/g MgO, which is ~0.6 wt % of the MgO particles and 0.45 wt % of the entire suspension. Suspensions with 0.6 mg/g MgO (0.06 wt % of MgO, 0.045 wt % of suspension) and 0.06 mg/g MgO (0.006 wt % of MgO, 0.0045 wt % of suspension) were also tested. These concentrations compare to the MgO suspensions investigated by Laarz et al.[4] and Kirby and Lewis[32] that use 6 and 4 mg/g MgO, respectively and is within the range of ADVA 190 to be added per weight of cement prescribed by the manufacturer (195–980 mL/100 kg cement).

For suspensions containing the comb-polymer, ADVA 190 was added to deionized water and stirred for 30 min before gradual addition of the MgO particles. For suspensions without comb-polymer, the particles were added to the water gradually with frequent shaking to produce a uniform suspension. MgO suspensions were kept stirring constantly after fabrication. Sonication for 5 min was applied for suspensions with comb-polymer to help prevent sedimentation after fabrication and suspensions were sonicated again for 5 min before testing.

The pH of the 0.46 vol. fraction MgO particles in deionized water was ~11.5, measured with a pH meter calibrated with buffer solution. The ADVA 190 comb-polymer had a pH of 4.5 in deionized water and MgO suspensions containing comb-polymer displayed a pH of 11.5. It has been reported that MgO particles have a positive charge at a pH of 11 but have a negative charge at a pH of 13.[11]

Zeta-potential measurements were carried out with a zeta-potential analyzer (Nanosizer nano-z, Malvern Instruments) applying the Smoluchowshi model. MgO particles of diameter 10 μm or less were dispersed in deionized water and filled disposable capillary cells with a syringe (DTS 1060, Malvern Instruments). The three samples tested were allowed to stir for 2 min before testing and had an equilibration time of 1 min at 25°C in order to measure the potential after the initial MgO hydration reaction, which occurs within 2 min for cement particles.[33] Low concentrations of MgO and comb-polymer were used to avoid noise interfering with the measurement in order to obtain the clearest zeta-potential possible.

UV–vis spectra were collected from centrifuged suspensions in order to determine the relative concentration of free comb-polymer by comparison with a calibration curve created from UV–vis spectra of comb-polymer solutions of known concentration (20, 10, 5, 1, 0.5, 0.25 mg/mL). Suspensions of narrow (6, 0.6, 0.06 mg/g comb-polymer) and wide distribution particles (6 mg/g comb polymer) were centrifuged for 5 mins at 1000 rpm. Particles settled at the bottom of the centrifuge tube and the water containing free comb-polymer (if any), was decanted and analyzed with UV–vis (Cary 60 UV–vis, 500–200 nm scan, dual beam). PAA absorption (at 200 nm wavelength) of the known concentration solutions used for calibration were correlated to the absorption of free comb-polymer from the different MgO suspensions in order to determine the approximate free comb-polymer concentrations in each suspension.

Shear rheometry (Anton Paar MCR 302) was performed one day after formation of the suspension. A stainless steel Couette fixture (27 mm in cylinder diameter, 1 mm gap, 19.35 mL sample volume) was used for all rheometry experiments. The suspension was poured into the Couette cup and then the inner cylinder was lowered and a solvent trap positioned to prevent the evaporation of water during testing. A 5 min wait time allowed the suspension to reach its equilibrium microstructure to reverse any effects of pouring. On the basis of particle size distributions and particle volume fraction, the equilibrium particle spacing for narrow distribution particles was estimated to be 3.3 μm while the spacing of wide distribution particles was estimated as 13.1 μm. Shear start-up tests were performed at a constant shear rate ($\dot{\gamma}$ = 0.001, 0.01, 0.1, or 1.0 s^{-1}) and the shear stress response was measured as a function of time. Each shear start-up test was conducted with a new sample, and shear stress data was collected over 200 s or more. Shear-ramp tests were conducted by measuring the shear stress over progressively increasing shear rates from 0.1 to 10 s^{-1} with 100 data points collected linearly. Creep experiments were performed with a constant shear stress of 10 Pa applied to the suspension for 500 s to measure the shear rate over time.

RESULTS

Zeta-Potential Measurements

The zeta-potential was recorded in counts per mV, with a peak at the highest intensity potential averaged over 50 runs at 8 s each. Alone, MgO particles (0.01 wt %) had a zeta-potential of 20.8 ± 5.71 mV. For the comb-polymer in water (0.01 wt %), zeta-potential was −24.2 ± 6.11 mV. When MgO particles and comb-polymer were combined, the zeta-potential was −17.1 ± 5.43 mV. Zeta-potential measurements were consistent with literature values for both diluted MgO suspensions[13] and cement particles[34] and confirms the adsorption of the comb-polymer on the MgO particle surfaces. Ferrari et al. observed the zeta-potential of MgO particles transition from a positive value (∼3.0 mV) to a negative value (∼−8.0 mV) upon addition of the comb-polymer.[6] This effect was also seen in Negele and Schneider's cement particle samples with a comb polymer.[34] For the MgO particles with comb-polymer, the zeta-potential of −17.1 mV is considered to be near the agglomeration threshold of −15.0 mV,[35,36] with aggregates of 2–10 particles capable of forming.[35,36] From these results, it was concluded that polymer-induced steric repulsion between neighboring MgO particles exists because of comb-polymer adsorption on the MgO surface.

UV–Vis Spectroscopy of Free Comb-Polymer

Approximate concentrations of free comb-polymer were determined with a UV–vis spectroscopy calibration curve generated from aqueous comb-polymer solutions of known concentrations. The wide particle size distribution suspensions with 6 mg/g comb-polymer had a free comb-polymer concentration of 0.32 mg/g (5.3% of the total comb-polymer concentration) while the narrow size distribution suspensions had a free comb-polymer concentration of 0.31 mg/g (5.1% of the total comb-polymer concentration). Free comb-polymer was found to be negligible (below the detection limits of UV–vis) for the 0.6 and 0.06 mg/g narrow size distribution suspensions.

Shear Rheometry of Narrow Distribution Suspensions

Rheometry experiments were conducted to observe shear-induced jamming behavior in concentrated MgO suspensions with and without adsorbed comb-polymer. Results from the suspensions created from the narrow particle size distribution MgO are discussed first. The influence of the adsorbed comb-polymer on the suspension's rheological behavior is examined through the presence of overshoots in the shear stress data.

Results from steady-state shear tests are presented in Figure 3 for suspension samples with and without comb-polymer. Both samples displayed shear stress overshoots during constant applied shear rates of 0.001, 0.01, 0.1, and 1.0 s^{-1}. The temporal occurrence of overshoots displayed a clear dependence on shear rate, with overshoots forming more quickly at greater applied shear rates. Additionally, the presence of comb-polymer further decreased the formation time. For example, the overshoot at 1.0 s^{-1} for the comb-polymer stabilized suspension [Figure 3(b)] appeared to occur in less than 0.1 s while the 1.0 s^{-1} overshoot for the polymer-free suspension occurred at ∼0.15 s^{-1} [Figure 3(a)]. Magnitudes of the overshoot were also dependent on the presence of comb-polymer. The suspension

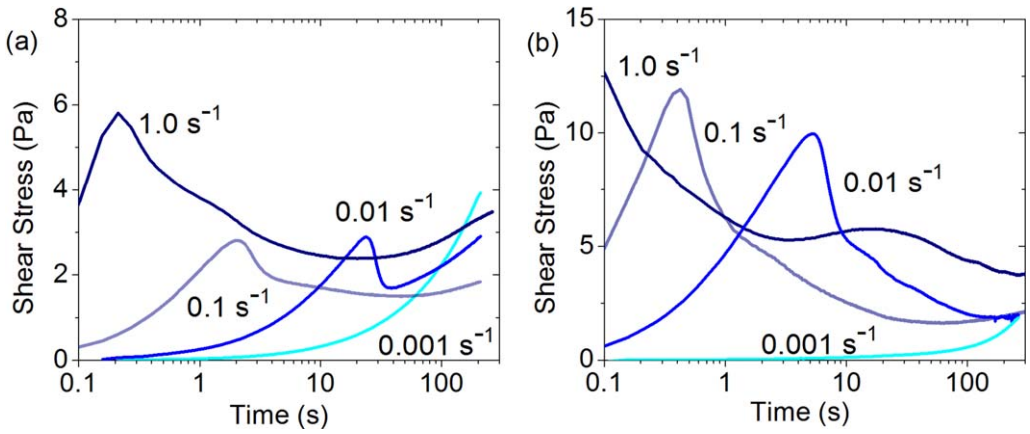

Figure 3. Shear start-up tests at different constant shear rates for narrow size distribution suspensions (a) without comb-polymer and (b) with 6 mg/g comb-polymer. [Color figure can be viewed in the online issue, which is available at wileyonlinelibrary.com.]

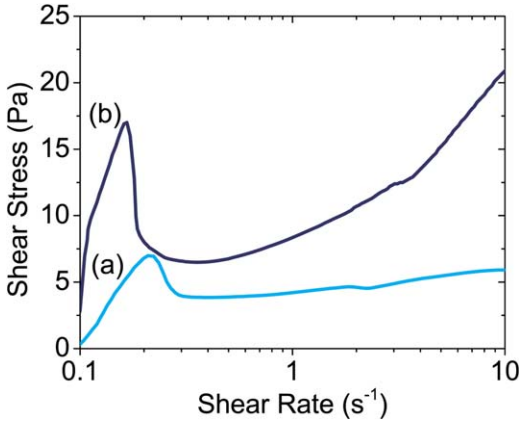

Figure 4. Flow curves for narrow size distribution suspensions (a) without comb-polymer and (b) with 6 mg/g comb-polymer. [Color figure can be viewed in the online issue, which is available at wileyonlinelibrary.com.]

with comb-polymer has overshoot magnitudes that range from 10 to 13 Pa while the polymer-free suspension displayed peak heights of 3–6 Pa. Beyond the stress overshoots, the polymer-free suspension displayed strong shear thickening behavior after the overshoot. In contrast, the suspension with comb-polymer appeared to formed shear stress plateaus (only slightly shear thickening) after 100 s for all shear rates tested except the 0.001 s^{-1}, which had not reached the overshoot by the end of the experiment.

Shear ramp experiments were also performed on the narrow particle size suspensions (Figure 4). Similar to the results in Figure 3, the suspension with comb-polymer displayed overshoot magnitudes ~10 Pa greater than the polymer-free suspensions. Indeed, over the entire shear rate range tested, the comb-polymer stabilized suspension exhibited greater stress magnitudes than the polymer-free suspension. At high shear rates, significant shear thickening was observed for the suspension with comb-polymer while the polymer-free suspension forms an approximate plateau.

Shear start-up and shear ramp experiments were also performed for samples of the narrow particle size distribution suspensions containing varying concentrations of comb-polymer (6, 0.6, 0.06, and 0.0 mg/g MgO; see Figure 5). In the shear start-up tests [Figure 5(a)], all concentrations display stress overshoots before 1.0 s, and overshoot magnitudes increase with comb-polymer concentration. Overshoot magnitudes follow the same trend in the flow curves [Figure 5(b)] with the 6 mg/g ADVA suspension having the greatest magnitude at ~17.5 Pa.

Overall, the presence of comb-polymer in the narrow particle size distribution suspensions leads to accelerated overshoot formations and increased overshoot magnitudes. Postovershoot shear thickening behavior was also more evident for comb-polymer stabilized suspensions.

Shear Rheometry of Wide Distribution Suspensions

Shear start-up experimental results for wide particle size distribution suspensions with and without comb-polymer are shown in Figure 6. The polymer-free suspensions demonstrate accelerated overshoot formation with increasing applied shear rate, similar to the data observed for the polymer-free narrow particle size distribution suspensions [Figure 3(a)]. Interestingly, as seen in Figure 6(b), the presence of comb-polymer in the suspension appears to significantly delay overshoot formation, which is an opposite trend from what was observed for the narrow distribution suspensions in Figure 3(b). An additional difference is the presence of multiple overshoots in Figure 6(b) as compared to Figure 3(b). Similar to the narrow distribution suspensions, the presence of comb-polymer in the wide distribution samples generally increased the overshoot magnitude as compared with the polymer-free overshoots.

In the shear ramp experiments (Figure 7), the polymer-free suspensions displayed a single overshoot followed by a weakly thickening stress plateau, similar in response and magnitude to the response of the narrow particle size distributions in Figure 4. However, in the presence of comb-polymer, the wide distribution suspensions show multiple stress overshoots with increasing shear rate before strongly shear thickening. This is in clear contrast to the single overshoot behavior during the same experiment with the narrow particle size distribution.

Overall, the suspensions containing the wide distribution MgO particles, which are believed to be more representative of actual

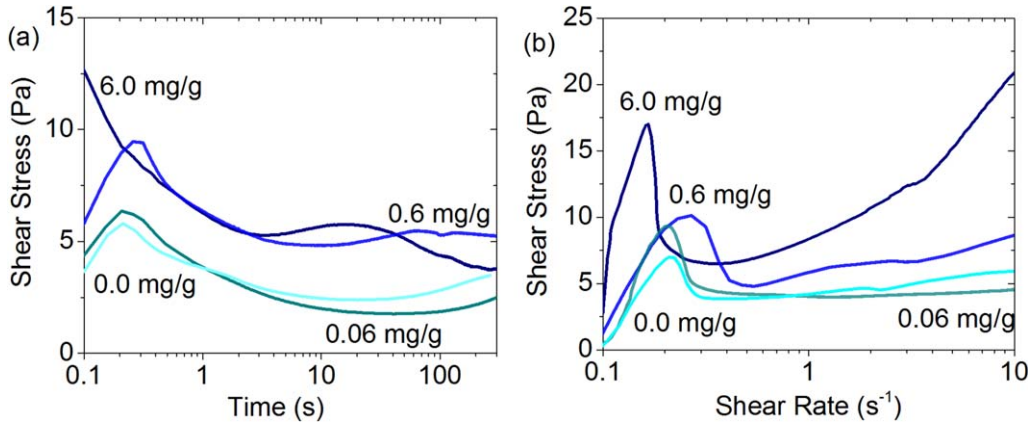

Figure 5. Shear tests for various concentrations of comb-polymer in narrow distribution size suspensions: (a) shear start-up tests at $\dot{\gamma} = 1.0\ s^{-1}$ and (b) shear ramp tests. [Color figure can be viewed in the online issue, which is available at wileyonlinelibrary.com.]

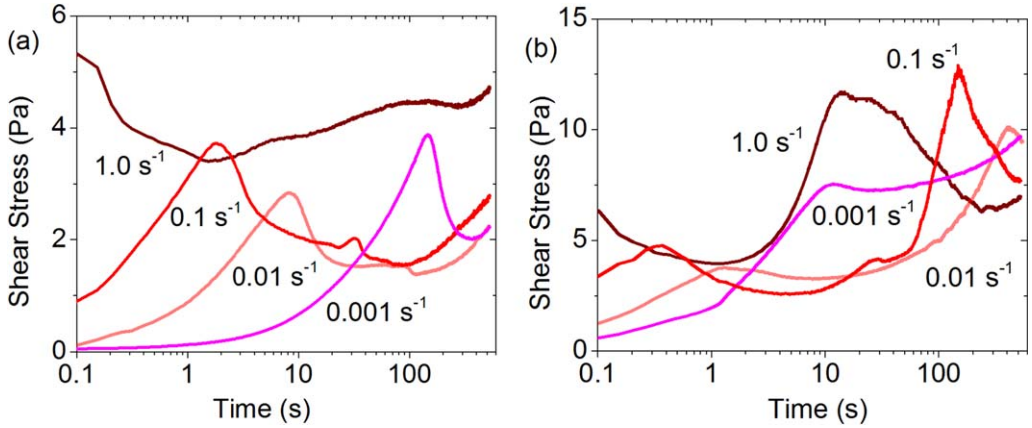

Figure 6. Shear start-up tests at different constant shear rates for wide size distribution suspensions (a) without comb-polymer and (b) with 6 mg/g comb-polymer. [Color figure can be viewed in the online issue, which is available at wileyonlinelibrary.com.]

cement mixtures, display very different rheological behavior in the presence of comb-polymer as compared to the suspensions containing the narrow distribution MgO particles. Delayed overshoot formation is observed and the development of multiple overshoots during shearing to large strain magnitudes or increased strain rates.

Creep Experiments of Narrow and Wide Particle Size Distribution Suspensions

Creep experiments were conducted on the four suspension samples—narrow and wide MgO distributions, with and without comb-polymer—to better simulate how these model cement suspensions may behave in service during pressure-driven flow during pumping and placement. Shown in Figure 8, the creep response for the polymer-free suspensions resulted in a two orders of magnitude increase in observed shear rates than the suspensions containing comb-polymer. Suspensions containing comb-polymer displayed creep response of similar shape (approximate plateau) while the polymer-free suspensions displayed strong variation in their curves. The wide particle size distribution suspension without comb-polymer displayed a maximum in its shear rate response over the time interval of the test while the narrow particle size distribution appeared to reach a high shear rate plateau.

Additional creep experiments were performed on samples of the narrow particle size distribution suspensions containing different concentrations of comb-polymer [see Figure 9]. In general, as the concentration of comb-polymer was increased, the observed final shear rate of the creep response was observed to strongly decrease.

DISCUSSION

Jamming in Both Narrow and Wide Particle Size Distribution Suspensions

The shear start-up and shear ramp rheometry results both displayed overshoots in the measured shear stresses, which are interpreted as indications of a changing colloidal suspension microstructure due to shear-induced jamming. As shown in the shear start-up tests in Figures 5(a) and 6, the overshoot formation time and overshoot magnitude were dependent on the particle size distribution and the inclusion of the comb-polymer. On the basis of the observed dependence of the shear-induced overshoot occurrences on the suspension's composition (narrow

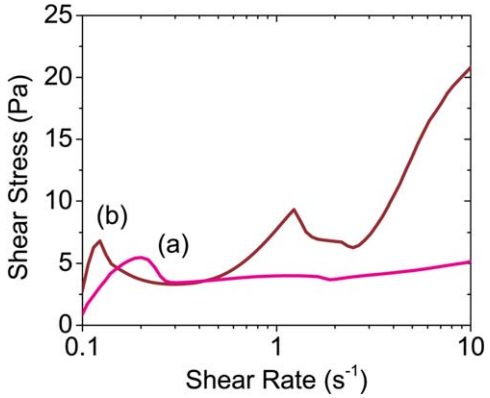

Figure 7. Flow curves from shear ramp experiments for wide size distribution suspensions (a) without comb-polymer and (b) with 6 mg/g comb-polymer. [Color figure can be viewed in the online issue, which is available at wileyonlinelibrary.com.]

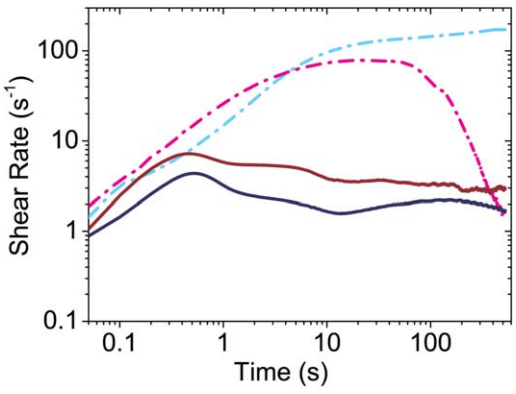

Figure 8. Creep experiments (τ = 10 Pa) for suspensions without comb-polymer (dotted line) and with 6 mg/g comb-polymer (line) and with a narrow particle size distribution (blue) or a wide distribution (red). [Color figure can be viewed in the online issue, which is available at wileyonlinelibrary.com.]

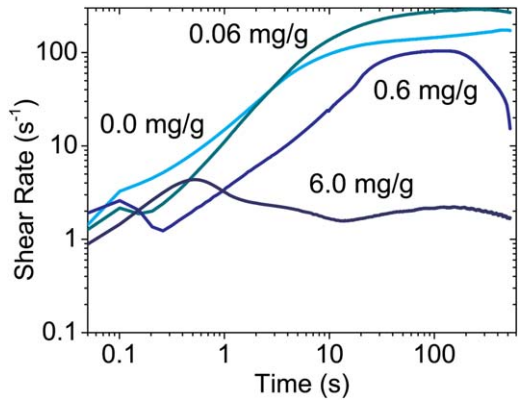

Figure 9. Creep experiments (τ = 10 Pa) for narrow distribution suspensions with varied concentrations of comb-polymer. [Color figure can be viewed in the online issue, which is available at wileyonlinelibrary.com.]

vs. wide MgO particle size distributions, with and without comb-polymer), a better understanding of the suspension's local microstructure and interparticle forces can be developed and is described in detail here.

For the concentrated suspensions examined herein (0.46 vol. fraction), particles are theorized to have been rearranged by the hydrodynamic force imposed on the fluid by the rotating inner cylinder of the Couette fixture. From the shearing, different particle microstructures formed and their morphologies depended on the particle sizes and comb-polymer concentration. Upon the initiation of a shear start-up experiment with a constant shear rate, shear thickening was observed, most likely resulting from particle convergence into a jammed, interlocked structure. As shearing progressed, the jammed microstructure appeared to rapidly deconstruct and remobilize, inferred by the observed shear thinning decrease in the shear stress, which resulted in the formation of a maximum in the stress response, or "overshoot."

Jamming overshoots occurred in all of the suspensions tested herein, narrow or wide particle size distributions, with or without comb-polymer. Low applied shear rates (e.g., 0.001 s^{-1}) exhibited delayed jamming, which is believed to be due to the weak hydrodynamic force applied to the colloid.[37] This affect leads to overshoots at timescales greater than 100 s, seen in the 0.001 s^{-1} overshoots in most shear start-up tests [Figures 3(a,b) and 6(a)]. Likewise, higher applied shear rates (e.g., 1.0 s^{-1}) displayed overshoots at earlier times due to the faster particle migration imparted by the stronger hydrodynamic forces of the shearing.[37] In the 1.0 s^{-1} trials, overshoots occurred before 0.3 s or developed so quickly that they were not able to be resolved by the experiment [Figure 5(a)]. The same overshoot dependency on shear rate has been reported for cement pastes,[27] which can be considered an analog of the suspensions discussed here. The overshoot temporal response in the shear ramp flow curves for the MgO suspensions [Figures (4 and 5)(b), and 7] also correlated with shear start-up tests through the observation of overshoots at low applied shear rates (2 s^{-1}). The early presence of overshoots in the flow curve is believed to have been the same indication of jamming as the overshoot in the shear start-up tests due to particle migration and particle collisions.[25]

Jamming phenomena have been explained through various colloidal microstructure theories, including particle caging[25] and force-chain theories,[21,38] but these are not specific to MgO-comb-polymer suspensions or cement pastes. On the basis of the differences in the particle size distribution and comb-polymer concentration, it is theorized that the comb-polymer contributed to (1) the creation of PEO-entangled particle networks in the narrow distribution suspensions or (2) the formation of hydroclusters of large particles with smaller particles trapped in the clusters in the wide distribution suspensions. Evidence for these ideas is described in the following sections.

Estimation of Polymer Chain Entanglement During Particle Jamming

To better understand the local conformation of adsorbed comb-polymer on the MgO particle surfaces, physical estimates for chain surface density and local side-chain concentration and entanglement were calculated for the 6 and 0.06 mg/g comb-polymer concentrations and the narrow and wide particle size distributions using theories from polymer brush theory[39] and polymer physics.[40]

A large side-chain surface density may impact chain entanglement on account of the close proximity of particles during jamming. Because of the negatively charged backbone of the comb-polymer chain, the backbone is most likely fully adhered to the particle surface (as illustrated in Figure 1), with the hydrophilic PEO side-chains extending into the surrounding fluid. Side-chains may be spaced depending on the particle size and comb-polymer concentration. Comb-polymer chain densities were calculated using the specific surface area of the MgO particles and assuming 95% absorption of comb-polymer to the MgO surface for the suspensions containing 6 mg/g comb-polymer concentrations and 100% absorption of comb-polymer to the MgO surface for the 0.6 and 0.06 mg/g concentration (based on UV–vis results). Specific surface area for these narrow size distribution suspensions was 357.2 m^2kg^{-1}, calculated from the following simplified Coulter counter size distribution: 0.5% of the particles were 1 μm in diameter, 2 μm (10%), 4 μm (23.5%), 6 μm (50%), 10 μm (10%), and 30 μm (5.5%). The wide particle size distribution suspensions have a specific surface area of 13.0 m^2kg^{-1} based on the abbreviated Coulter counter particle size distribution: 10 μm (10%), 50 μm (10%), 75 μm (10%), 107 μm (20%), 200 μm (31%), and 300 μm (20%). Chain surface density (σ) was calculated by dividing the number of comb-polymer chains by the total surface area of particles based on the mentioned sized distributions. Each comb-polymer molecule contained an estimated 15 total side-chains along the 5000 g mol^{-1} backbone chain.[4,6,11] Side-chain densities along with comb-polymer chain densities are reported in Table I. These values are not absolute portrayals of actual densities (as such large values of side-chain surface density are not realistic); instead, these values will be used comparatively to develop a qualitative understanding of the impact of particle size and comb-polymer concentration on the side-chain entanglement interactions between jammed particles.

Side-chain conformations of fully extended and fully coiled were considered as the limits of chain conformation. The side-

Table I. Calculations of C and the Physical Parameters Used to Calculate C for Both Narrow and Wide Particle Size Distribution Suspensions

	Narrow		Wide
Particle sizes (μm)	3.8 ± 2.5		108.9 ± 88.4
Comb-polymer concentration (Φ)	6 mg/g	0.06 mg/g	6.0 mg/g
Comb-polymer surface density (σ, chains/nm^2)	0.5	0.005	14
Side-chain surface density (σ, chains/nm^2)	7.2	0.08	204
C			
Fully coiled limit	124	1.3	3500
Fully extended limit	1.4	0.02	40

chain length for a fully extended all-trans conformation (L_{trans})[40]:

$$L_{trans}=3Nl_{bond}\sin\left(\frac{\theta}{2}\right), \quad (1)$$

where N is the number of monomers (N = 23 for a 1000 g mol^{-1} PEO side-chain), l_{bond} is 0.153 nm (the approximate length of a C—C bond in the backbone of a polymer chain), and θ is the bond angle of 112° for a chain in the all-trans conformation. From eq. (1), the fully extended side-chain length L_{trans} was found to be 8.8 nm. Side-chain arrangement and adsorption volume were also considered for a coiled chain configuration based on the radius of gyration for a polymer in good solvent with the Kuhn length of the monomer (a), 1.1 nm,[40] and the number of Kuhn monomers (N_{Kuhn})[40]:

$$L_{coiled} \approx R_g = aN_{Kuhn}^{3/5} \quad (2)$$

N_{Kuhn} was found by dividing the length of the chain by the Kuhn monomer molecular weight, 137 g mol^{-1}.[40] From eq. (2), the fully coiled side-chain length was estimated to be 3.6 nm.

To determine the likelihood of side-chain entanglement during jamming, local side-chain concentration (C) was calculated using the Alexander-de Gennes model for polymer brushes grafted to a surface[41] and compared to the critical entanglement concentration (C^*). Since grafted and adsorbed chains have been shown to have similar behavior in good solvent,[42] the grafted chain model was applied. Molecular dynamics simulations have employed the Alexander-de Gennes model or made variations of it for studying brush interactions.[43–47] This method is adopted here to approximate the space-filling dimensions of the comb-polymer side-chains that extend from the MgO particle's surface and ultimately to estimate the local concentration of side-chains existing between neighboring jammed particles.

To aid in the prediction of entanglement, a physical model was developed (see Figure 10). In the model, a 1.5 L interaction zone exists between neighboring jammed particles, which results in a 0.5 L overlap between opposing side-chains. Each side-chain is assumed to have an effective width of x, equivalent to the estimated monomer width for the extended all-trans chain (x_{trans} = 0.38 nm) or the radius of gyration for the fully coiled chain (x_{coiled} = 3.6 nm). Volume per chain is then found by use of the following equation:

$$V_{chain}=Lx^2, \quad (3)$$

with L as the length of the chain, either L_{trans} or L_{coiled}. This is similar to Alexander-de Gennes treatment,[41] only here the grafting distance is replaced by x_{trans} or x_{coiled} as it is assumed that chains do not fill all space and instead will be separated by interpenetrating chains from a neighboring particle. The effective number of chains per two surfaces in the interaction zone (N_{chain}) was determined from the chain surface density:

$$N_{chain}=2\sigma(1.5L)^2 \quad (4)$$

Local side-chain concentration in the 1.5 L volume element is calculated through a ratio of the volume of chains over the volume of the 1.5 L box (V):

$$C=\frac{V_{chain}N_{chain}}{V}. \quad (5)$$

The value of C is the volume fraction of side-chains within the interaction zone for the narrow or wide particle size distribution (see Table I). The critical overlap concentration, C^*, was assumed to be unity, as the threshold for side-chain entanglement is when chains are close-packed within the bounding volume. Therefore for $C >> 1$, there is likely to be entanglement between opposing side-chains while for $C \leq 1$, no significant side-chain entanglement is expected to occur.

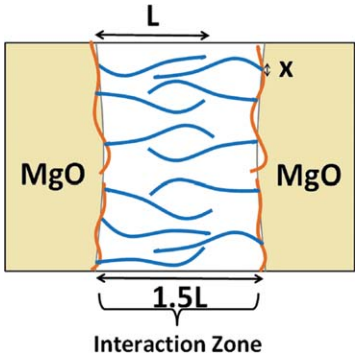

Figure 10. Interaction zone between two particles separated by 1.5 L with a 0.5 L penetration between chains; extended chains are shown although the model is applied for both fully extended and fully coiled chain conformations. [Color figure can be viewed in the online issue, which is available at wileyonlinelibrary.com.]

As shown in Table I, $C >> 1$ was calculated for the narrow particle size distribution suspensions containing 6 mg/g comb-polymer (95% adsorbed comb-polymer) for the fully coiled limit and the fully extended limit had $C \geq 1$. Therefore, side-chain entanglement during jamming is most likely possible within this suspension. On the other hand, the suspension containing a lower concentration of comb-polymer (0.06 mg/g, narrow size suspensions, 100% adsorbed) resulted in $C << 1$ for the extended limit and $C \geq 1$ for the coiled limit, and thus side-chain entanglement is unlikely to occur for this suspension. Additionally, wide particle size suspensions (95% adsorbed comb-polymer) are also expected to have side-chain entanglement during jamming due to the $C >> 1$ values shown in Table I.

Network Formation for Narrow Particle Size Distribution Suspensions

Narrow particle size distribution suspensions displayed a single shear stress overshoot peak with greater peak magnitudes and accelerated peak onset when comb-polymer was used in the suspension (Figure 3). Following the overshoot, plateau-like behavior was observed for the suspension containing comb-polymer. However, for the polymer-free suspension, a second shear thickening regime was observed, which may indicate the onset of a second jamming transition. Increased side-chain entanglement is believed to have brought about higher overshoots for high comb-polymer concentration (6 mg/g) suspensions. The lowest comb-polymer concentration, 0.06 mg/g, may not have side-chain entanglement due to $C << C^*$ for the lower limit (coiled) and C only slightly above unity for the upper limit (all-trans) of chain conformation (Table I) and thus had a smaller overshoot magnitude. Creep tests (Figure 9) also confirm the difference between adsorbed comb-polymer particles and bare particles through the measured decrease in shear rate for increased comb-polymer concentration.

As described previously, the stress overshoot is interpreted as an indication of a shear-induced jamming transition within the suspension. Side-chain interpenetration may occur during the jam and lead to the subsequent formation of a networked microstructure of particles and entangled polymer. Local side-chain concentration surpassed the critical entanglement concentration ($C >> 1$) for the 6 mg/g suspension but not the 0.06 mg/g concentration (Table I). A lack of entanglement in the 0.06 mg/g suspension may be responsible for the nearly-identical overshoot behavior to suspensions without comb-polymer [Figure 5(a)]. This overshoot behavior may also explain how side-chain entanglement results in high overshoot magnitudes due to friction forces interpenetrating or entangled side-chains[48] and overshoot peak height may serve as an indication of entanglement strength.[15] Additional evidence for network formation in the narrow size distribution suspensions with high concentrations of comb-polymer was also obtained from creep experiments. In the creep experiment, the high shear rates for the small side-chain concentration suspension (0.06 mg/g, Figure 9) may serve as a sign of low chain friction and perhaps also poor network strength between particles. Therefore, the absence of particle networks is likely.

The relationship between comb-polymer concentration and increased jamming overshoots may be applied to cement processing. Increased shear stresses from jams may hinder cement paste flow due to the friction between comb-polymer-adsorbed cement particles that grow with greater comb-polymer concentrations. Jamming overshoot shear stress may be reduced through use of lower comb-polymer concentrations, which is seen in the smaller overshoot peak of 0.6 and 0.06 mg/g in shear start-up tests [Figure 5(a)] and shear ramp tests [Figure 5(b)] with ~7 Pa less shear stress than the 6 mg/g suspension. Creep tests (Figure 9) also showed that the 0.6 mg/g suspension is better suited for pressure-driven flow than the 6 mg/g because the increased shear rate indicated that the suspension can undergo shearing at faster rates under applied stress ($\tau = 10$ Pa). UV–vis results indicated that a small amount of free comb-polymer (~5%) was present in the suspensions containing the highest concentration of comb-polymer (6 mg/g). These suspensions displayed the greatest magnitude of jamming so it may be possible that the presence of free comb-polymer in the suspension facilitates additional entanglement between comb-polymer adsorbed onto neighboring particles. To confirm this effect, experiments are currently underway to measure the rheological behavior of suspensions containing controlled amounts of free polymer in addition to adsorbed comb-polymer.

Hydrocluster Theory for Wide Particle Size Distribution Suspensions

Similar to the narrow particle size distribution suspensions, the wide particle size distribution samples displayed overshoots with overall greater peak magnitudes when comb-polymer was present as compared to the polymer-free suspensions (Figure 6). Suspensions with comb-polymer also exhibited multiple overshoots in both shear start-up and flow curve experiments (Figures 6 and 7) like the shear thickening single overshoot peaks of polymer-free suspensions but at different time scales. Creep tests (Figure 8) measured higher shear rates for the comb-polymer suspension than the narrow size distribution suspension, which also suggests a difference in flow behavior.

The observed increase in overshoot magnitude in comb-polymer containing suspensions is consistent with the hypothesized interpenetration and entanglement during jamming of the hydrophilic side-chains of the comb-polymer discussed in the previous section. In this case, the wide particle size distribution of the MgO particles in the suspension would most likely result in a microstructure composed of particle hydroclusters. Hydroclusters are aggregates of particles of various sizes, with the smaller particles filling the interstitial space between larger particles.[22] The hydrocluster structures proposed herein were most likely aggregates of 2–10 particles of various sizes as determined from zeta-potential measurements close to −15.0 mV.[35,36]

The presence and potential interactions between hydrophilic side-chains of the comb-polymer may also have contributed to the formation of hydroclusters by the entrapment of smaller particles. Decreased specific surface area for the wide size distribution suspension (13 m^2kg^{-1}) resulted in increased comb-polymer surface density and therefore the local surface concentration was significantly larger than narrow particle size suspensions. Because of the large particles (e.g., over half were 100 μm in diameter), the wide particle size distribution suspension was

also capable of side-chain entanglement for both fully extended and fully coiled chains due to $C >> 1$ (Table I), which may have kept smaller particles entangled to larger particles within the hydroclusters.

Interparticle Interactions

To assess the validity of the proposed microstructures of the comb-polymer stabilized suspensions, particle interaction potentials are discussed and compared to literature values for similar systems.

Steric interaction potentials were evaluated and analyzed to elaborate on the possibility of network and hydrocluster formation of the MgO particles with absorbed comb-polymer. The steric interaction potential between two spheres with attached polymer chains (φ_{steric}) is given by:

$$\Phi_{steric} = \frac{4\pi}{3} kTB_2c^2\left(\delta - \frac{S_o}{2}\right)^2\left(3a + 2\delta + \frac{S_o}{2}\right) \quad (6)$$

where k is Boltzman's constant, T is absolute temperature, B_2 is the second viral coefficient, c is the average mass concentration of segments of the stabilizing moieties in the adsorption layer, δ is the adsorption layer thickness, S_o is the distance of closest approach of particle-free particle surfaces, and a is the particle radius.[49] The only variable in eq. (6) capable of changing the sign of the interaction potential is the second viral coefficient, which has been reported as 9×10^{-7} mol g^{-2} for linear PEO in water.[50] Therefore, the steric interaction potential for the extended hydrophilic chains in the suspension can only be positive, indicating the exclusively repulsive nature of the steric forces at work.

Derjaguin–Landau–Verway–Overbeek (DLVO) calculations of the steric forces at work often predict repulsion between particles; however, for particles in the micrometer range an attractive well exists.[3,51] The repulsion from the steric forces, represented by c in eq. (6), is less for short chains attached to micrometer-sized particles,[4,51] which increases the likelihood of attraction between particles.[3,51] Furthermore, the energy minimum of the well decreases when larger volume fractions of particles are used.[49] It is proposed that for the comb-polymer stabilized suspensions investigated here, the shear-induced collisions and 0.46 particle volume fractions contributed to the formation of networks or hydroclusters through particles attracting due to the potential minimum in the suggested DLVO model.

Other than repulsive steric forces and attractive Van der Waals effects, electrostatic forces may also be present in the colloidal suspension from the MgO hydration[52] although their effects on the overall suspension particle interactions were minimal.[51] For the MgO suspensions investigated here, the electrostatic potential does not appear to significantly affect the suspensions as no external salts were added to the system.

Overall, the steric repulsion competed against Van der Waals attraction during the formation of various particle microstructures under shear. Particle hydroclusters formed on account of the largest particles in the wide particle size distribution being more prone to Van der Waals forces than the steric repulsion from the small, 1000 g mol^{-1} hydrophilic side-chains of the comb-polymer, as effective steric repulsion diminished for larger particles. The attractive minimum is also believed to aid the formation of networks in the narrow size distribution suspensions.

SUMMARY AND IMPLICATIONS

Altogether, the particle microstructure determines the rheological response of the concentrated MgO suspensions through the influence of the hydrodynamic shear force as well as the hypothesized particle interactions and chain entanglement. Particle jamming transitions, observed as a shear stress overshoot in rheometry experiments, directly depended on the MgO particle size distribution and the comb-polymer concentration in the suspensions. For suspensions containing a narrow particle size distribution of MgO and a relatively high concentration of comb-polymer (>0.06 mg/g), the overshoot magnitude may indicate the strength of chain entanglements that bind particles together in a network microstructure. Small concentrations of comb-polymer are postulated to have reduced network strength due to fewer side-chains per particle. In suspensions composed of wide particle size distribution particles, the presence of the absorbed comb-polymer at relatively high concentrations was believed to entangle small particles into hydroclusters while larger particles were attracted by Van der Waals forces. Two overshoots were observed at different shear rates for the comb-polymer containing wide particle distribution suspensions, possibly indicating repeated hydrocluster jamming with increased shear deformation. Additionally, the small amount of free comb-polymer in suspensions containing the greatest comb-polymer concentration (6 mg/g) may contribute to the enhanced jamming behavior; however, future work is needed to confirm this idea.

The particle interactions and shear testing conditions simulated the conditions for cement processing and can be used to understand jamming in cement pastes. Jamming transitions lower the workability of the cement paste at the moment of the jam. Furthermore, wide particle size distribution suspensions, which more accurately model cement in their particle sizes, display evidence of multiple jamming transitions over time. Therefore, particle jamming may repeat in cement pastes and continue to be an obstacle to cement mixing and placement. As seen in the MgO suspensions, these jams in the particles may be adjusted or mitigated by minimizing the comb polymer concentration, which decreases the side-chain surface density and therefore lowers the amount of side-chain entanglement. By reducing comb-polymer concentration in cement pastes, particle networks or hydroclusters may not form as readily, allowing for easier cement processing and flow.

ACKNOWLEDGMENTS

This material is based upon work supported by the National Science Foundation Graduate Research Fellowship Program under Grant No. DGE-1333468.

REFERENCES

1. Flatt, R. J.; Martys, N.; Bergström, L. *MRS Bull.* **2004**, *29*, 314.

2. Kirby, G. H.; Lewis, J. A. *J. Am. Ceram. Soc.* **2004**, *87*, 1643.
3. Lewis, J. A.; Matsuyama, H.; Kirby, G.; Morissette, S.; Young, J. F. *J. Am. Ceram. Soc.* **2000**, *13*, 1905.
4. Laarz, E.; Kauppi, A.; Andersson, K. M.; Kjeldsen, A. M.; Bergstrom, L. *J. Am. Ceram. Soc.* **2006**, *89*, 1847.
5. Bedrov, D.; Smith, G. D.; Chun, B.-W. *Eur. Polym. J.* **2010**, *46*, 2129.
6. Ferrari, L.; Kaufmann, J.; Winnefeld, F.; Plank, J. *Cem. Concr. Res.* **2011**, *41*, 1058.
7. Kjeldsen, A. M.; Flatt, R. J.; Bergström, L. *Cem. Concr. Res.* **2006**, *36*, 1231.
8. Marchon, D.; Sulser, U.; Eberhardt, A.; Flatt, R. J. *Soft Matter.* **2013**, *9*, 10719.
9. Larson, R. G. In The Structure and Rheology of Complex Fluids; Oxford University Press: New York, **1999**; pp. 263–322.
10. Flatt, R. J.; Schober, I.; Raphael, E.; Plassard, C.; Lesniewska, E. *Langmuir* **2008**, *25*, 845–855.
11. Houst, Y. F.; Bowen, P.; Perche, F.; Kauppi, A.; Borget, P.; Galmiche, L.; Le Meins, J.-F.; Lafuma, F.; Flatt, R. J.; Schober, I.; Banfill, P. F. G.; Swift, D. S.; Myrvold, B. O.; Petersen, B. G.; Reknes, K. *Cem. Concr. Res.* **2008**, *38*, 1197–1209.
12. Kauppi, A.; Andersson, K. M.; Bergström, L. *Cem. Concr. Res.* **2005**, *35*, 133.
13. Flatt, R. J.; Houst, Y. F. *Cem. Concr. Res.* **2001**, *31*, 1169.
14. Moller, P. C. F.; Mewis, J.; Bonn, D. *Soft Matter.* **2006**, *2*, 274.
15. Srivastava, S.; Shin, J. H.; Archer, L. A. *Soft Matter.* **2012**, *8*, 4097.
16. Ballesta, P.; Koumakis, N.; Besseling, R.; Poon, W. C. K.; Petekidis, G. *Soft Matter* **2013**, *9*, 3237.
17. Bertrand, E.; Bibette, J.; Schmitt, V. *Phys. Rev. E* **2002**, *66*, 060401.
18. Laurati, M., Egelhaaf, S. U.; Petekidis, G. J. *J. Rheol.* **2011**, *55*, 673.
19. Malkin, A. Y. *J. Nonnewton. Fluid Mech.* **2013**, *192*, 48.
20. Mahmoudi, T.; Karimkhani, V.; Song, G. S.; Lee, D. S.; Stadler, F. J. *Macromolecules* **2013**, *46*, 4141.
21. Lootens, D.; Hébraud, P.; Lécolier, E.; Van Damme, H. *Oil Gas Sci. Technol.* **2004**, *59*, 31.
22. Cyr, M.; Legrand, C.; Mouret, M. *Cem. Concr. Res.* **2000**, *30*, 1477.
23. Kong, X.; Zhang, Y.; Hou, S. *Rheol. Acta* **2013**, *52*, 707.
24. Pasquino, R.; Nicodemi, F.; Vanzanella, V.; Alfani, R.; Grizzuti, N. *Rheol. Acta* **2013**, *52*, 395.
25. Rogers, S.; Vlassopoulos, D.; Callaghan, P. *Phys. Rev. Lett.* **2008**, *100*, 128304.
26. Fontani, G.; Gaspari, R.; Spencer, N. D.; Passerone, D.; Crockett, R. *Langmuir* **2013**, *29*, 4760.
27. Jayasree, C.; Murali Krishnan, J.; Gettu, R. *Mater. Struct.* **2010**, *44*, 929.
28. Coussot, P.; Nguyen, Q. D.; Huynh, H. T.; Bonn, D. *J. Rheol.* **2002**, *46*, 573.
29. Roussel, N.; Lemaître, A.; Flatt, R. J.; Coussot, P. *Cem. Concr. Res.* **2010**, *40*, 77.
30. Banfill, P. F. G. *Rheol. Rev.* **2006**, 61.
31. Luo, Y.; Ran, Q.; Wu, S.; Shen, J. *J. Appl. Polym. Sci.* **2008**, *109*, 3286.
32. Kirby, G. H.; Lewis, J. A. *J. Am. Ceram. Soc.* **2004**, *87*, 1643.
33. Nägele, E. *Cem. Concr. Res.* **1986**, *16*, 853.
34. Nägele, E.; Schneider, U. *Cem. Concr. Res.* **1988**, *18*, 257.
35. Schramm, L. L. In Emulsions, Foams, and Suspensions: Fundamentals and Applications, Wiley and Sons: Weinheim, Germany; **2005**; pp. 117–154.
36. Riddick, T. M. Control of Colloid Stability Through Zeta-Potential; Livingston: New York, **1968**.
37. Stokes, J. R.; Telford, J. H. *J. Nonnewton. Fluid Mech.* **2004**, *124*, 137.
38. Lyon, M. K.; Mead, D. W.; Elliott, R. E.; Leal, L. G. *J. Rheol.* **2001**, *45*, 881.
39. McCrum, N. G.; Buckley, C. P.; Bucknall, C. B. Principles of Polymer Engineering, 2nd ed.; Oxford University Press: New York, **2003**; pp 45–48.
40. Rubinstein, M.; Colby, R. H. Polymer Physics; Oxford University Press: New York, **2005**; pp 51–55.
41. Léger, L.; Raphaël, E.; Hervet, H. In Advances in Polymer Science; Springer-Verlag: Berlin, **1999**; Vol. *138*, pp 185–225.
42. Kreer, T.; Mu, M. H.; Binder, K.; Klein, J. *Langmuir* **2001**, *17*, 7804.
43. Binder, K.; Milchev, A. *J. Polym. Sci. Part B: Polym. Phys.* **2012**, *50*, 1515.
44. Zhao, B.; Brittain, W. J. *Prog. Polym. Sci.* **2000**, *25*, 677.
45. Doyle, P. S.; Shaqfeh, E. S. G.; Gast, A. P. *Macromolecules* **1998**, *31*, 5474.
46. Galuschko, A; Spirin, L.; Kreer, T.; Johner, A; Pastorino, C.; Wittmer, J.; Baschnagel, J. *Langmuir* **2010**, *26*, 6418.
47. Spirin, L.; Galuschko, A; Kreer, T.; Johner, A; Baschnagel, J.; Binder, K. *Eur. Phys. J. E. Soft Matter.* **2010**, *33*, 307.
48. Wang, S.-Q.; Wang, Y.; Cheng, S.; Li, X.; Zhu, X.; Sun, H. *Macromolecules* **2013**, *46*, 3147.
49. Berg, J. C. In An Introduction to Interfaces and Colliods: A bridge to Nanoscience; World Scientific: Singapore, **2010**; pp 525–615.
50. Striolo, A.; Prausnitz, J. M. *Polymer (Guildf).* **2001**, *42*, 4773–4775.
51. Yoshioka, K.; Sakai, E.; Daimon, M.; Kitahara, A. *J. Am. Ceram. Soc.* **1997**, *80*, 2667.
52. Nägele, E. *Cem. Concr. Res.* **1987**, *17*, 573.